A Comparative Study on Photovoltaic MPPT Algorithms Under EN50530 Dynamic Test Procedure

Xingshuo Li, *Member, IEEE*, Huiqing Wen, *Senior Member, IEEE*, Yihua Hu, *Senior Member, IEEE*, Yang Du, *Member, IEEE*, and Yong Yang, *Senior Member, IEEE*

***Abstract*—Dynamic performance of maximum power point tracking (MPPT) algorithms is important to ensure high-power output under practical operating conditions. In this article, after reviewing three dynamic test procedures, including stepped operation procedure, day-by-day operation procedure, and EN50530 dynamic test procedure, three typical MPPT algorithms such as the fixed-step-size perturb and observe (P&O), variable-step-size incremental conductance, and hybrid-step-size beta method are evaluated experimentally under the EN50530 dynamic test procedure. Two dynamic EN50530 test sequences are adopted for the performance evaluation to cover different irradiance changing conditions. The PV model for EN50530 dynamic test sequences is built, and the effects of wrong-step changes by using three MPPT algorithms are analyzed systematically. The experimental comparison of three MPPT algorithms in terms of the tracking routines, accumulated energy, and tracking efficiency is presented. The research shows that the 0.5% fixed-step-size P&O may fail to track the MPP due to the tracking drift, whereas the beta algorithm exhibits the highest tracking efficiency under both dynamic sequences. The average tracking efficiency improvement of the beta algorithm compared with other two algorithms are experimentally measured as 24.2% and 18.8%, respectively.**

***Index Terms*—Dynamics, EN50530 dynamic test procedure, maximum power point tracking (MPPT), photovoltaic (PV) system, tracking efficiency.**

I. Introduction

As the core technique in extracting the maximum possible power from the photovoltaic (PV) power systems, maximum power point tracking (MPPT) has gained wide attention and intensive research works recently. Until now, many MPPT techniques have been proposed with different merits in improving the performance of the actual power output [1], [2]. Considering that these MPPT techniques are usually tested under difference conditions in terms of PV modules, converter topologies, controllers, irradiation or temperature changing parameters, and load conditions, thus, a comprehensive performance evaluation of these MPPT algorithms under a well-defined test procedure becomes essential. For the steady-state performance evaluation, it is easy to conduct the experimental comparison by unifying the test conditions, such as irradiance, temperature, and loads. However, for dynamic performance evaluation, it becomes challenging for the performance evaluation considering more complicated environmental conditions and experimental parameters. Thus, in order to give a useful guide for MPPT algorithm selection under a specific working condition, a unified dynamic test procedure should be selected in order to make a fair dynamic performance comparison among different MPPT algorithms quantitatively.

Table I summarizes main MPPT dynamic test procedures, which can be classified into three categories according to their test requirements, features, and key parameter setting: stepped dynamic test procedure [3]–[6], day-by-day dynamic test procedure [7]–[9], and EN50530 dynamic test procedure [10]–[17]. Detailed discussion about the three MPPT dynamic test procedures will be presented as follows.

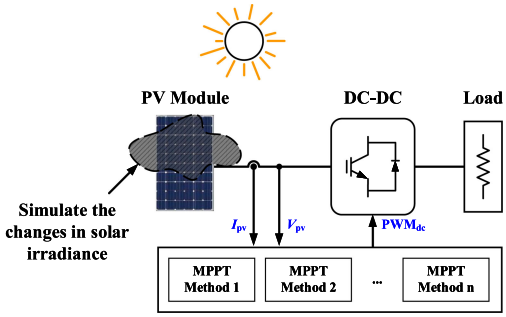

Fig. 1. System configuration of stepped dynamic test procedure.

A. Stepped Dynamic Test Procedure

As shown in Fig. 1, with this dynamic test procedure, only one unified power interface is required and main test conditions

Manuscript received May 5, 2020; revised August 13, 2020; accepted September 11, 2020. Date of publication September 15, 2020; date of current version November 20, 2020. This work was supported in part by the Research Development Fund of XJTLU under Grants RDF-16-01-10 and RDF-17-01-28, in part by the Research Enhancement fund of XJTLU under Grant REF-17-01-02, in part by the Research Start Fund of Nanjing Normal University under Grant 184080H202B232, in part by the Suzhou Prospective Application Programme under Grant SYG201723, and in part by the XJTLU Key Programme Special Fund under Grants KSF-A-08, KSF-E-13, and KSF-T-04. Recommended for publication by Associate Editor Prof. S. Mekhilef. *(Corresponding author: Huiqing Wen.)*

Xingshuo Li is with Nanjing Normal University, Nanjing 210023, China (e-mail: xingshuo.li@njnu.edu.cn).

Huiqing Wen is with the Xi'an Jiaotong-Liverpool University, Suzhou 215123, China (e-mail: Huiqing.Wen@xjtlu.edu.cn).

Yihua Hu is with the University of York, York YO10 5DD, U.K. (e-mail: yihua.hu@york.ac.uk).

Yang Du is with the College of Science and Engineering, James Cook University, QLD 4870, Australia (e-mail: yang.du@jcu.edu.au).

Yong Yang is with the School of Rail Transportation, Soochow University, Suzhou 215131, China (e-mail: yangy1981@suda.edu.cn).

Color versions of one or more of the figures in this article are available online at https://ieeexplore.ieee.org.

Digital Object Identifier 10.1109/TPEL.2020.3024211

TABLE I
COMPARISON OF MPPT DYNAMIC TEST PROCEDURES

Method	Accuracy	Test Time	Converter number	Test-bench Complexity	Test-bench Cost	System Cost-Effectiveness	References
Stepped dynamic test procedure	Middle	Short	One	Simple	Low	Middle	[3–6]
Day-by-day dynamic test procedure	High	Long	Depends	Complex	High	Middle	[7–9]
EN50530 dynamic test procedure	High	Short	One	Simple	Middle	High	[10–15]

including the load resistance or the solar irradiance are changing in a manner of stepped stairs so that the tracking speed of these algorithms in relocating the new MPP will be evaluated.

This dynamic test procedure shows the advantages of cost-effective and simple implementation.

Thus, it is currently the most widely used procedure for MPPT dynamic performance evaluation. However, due to the test setting, the stepped dynamic test procedure may not reflect the actual dynamic performance of MPPT algorithms [7].

B. Day-by-Day Dynamic Test Procedure

Compared with the stepped dynamic test procedure, the day-by-day dynamic test procedure is closer to the real working conditions, thus it is more accurate for the MPPT dynamic performance evaluation.

In [7], with the same PV modules and power converters as the test bench, two different MPPT algorithms were evaluated within the same period.

Specifically, totally 15 days with 8 h per day are used for the evaluation. Although the day-by-day dynamic test procedure is capable of providing a fair comparison among different MPPT algorithms, a large number of PV modules and power converters are required for building the test bench. Specifically, as shown in Fig. 2, the number of power converters in the test bench should be set the same as the number of MPPT algorithms for the performance evaluation. With this dynamic test procedure, the cost of the test bench is high. Furthermore, the corresponding testing time is also long. Therefore, this dynamic test procedure is not cost-effective in terms of both the test bench hardware and the demanding test time [8].

C. EN50530 Dynamic Test Procedure

In order to overcome the drawbacks of the aforementioned dynamic test procedures, EN50530 dynamic test procedure is proposed, which is regarded as a more realistic approach for the MPPT dynamic performance quantitative evaluation [10]–[12]. Compared to the stepped dynamic test procedure with stepped irradiance changes setting, EN50530 dynamic test procedure adopts slope irradiance changes setting, which is closer to the real working conditions for PV systems. Fig. 3 demonstrates the system configuration of EN50530 dynamic test procedure. From Fig. 3, it can be seen that the PV module is replaced by the PV emulator and only one power converter is required for the evaluation of several MPPT algorithms, which is cost-effective. Furthermore, the experimental evaluations can be conducted under indoor environment, which is convenient. Besides, the

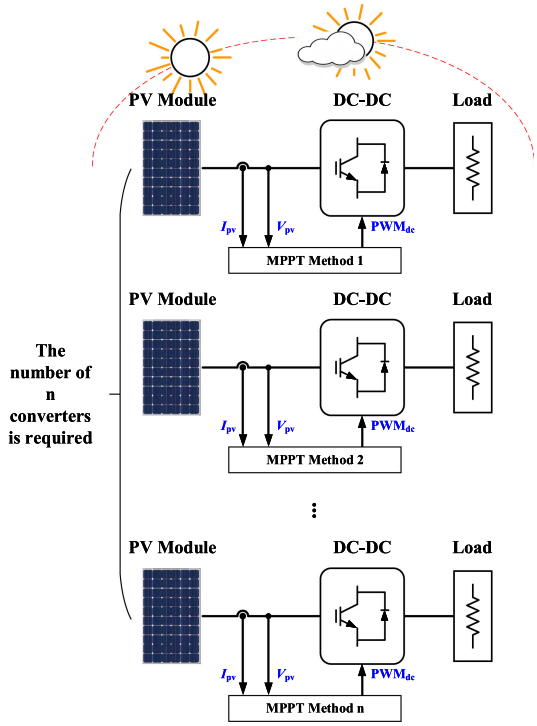

Fig. 2. System configuration of day-by-day dynamic test procedure.

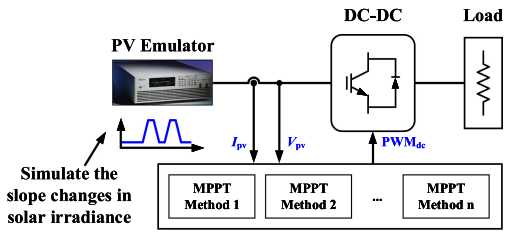

Fig. 3. System configuration of EN50530 dynamic test procedure.

test time can be regulated within several hours, which greatly simplified the practical implementation for the experimental evaluation.

So far, several articles have discussed the MPPT evaluation by using the EN50530 dynamic test procedure [10]–[14]. However, only basic MPPT algorithms, including the perturb and observe (P&O) and incremental conductance (INC) algorithm with fixed-step size, were discussed and evaluated by following the EN50530 dynamic test procedure. Considering the rapid advancement of PV MPPT algorithms [18], the evaluation in [10]–[12], and [19] is insufficient and unable to give a useful guideline

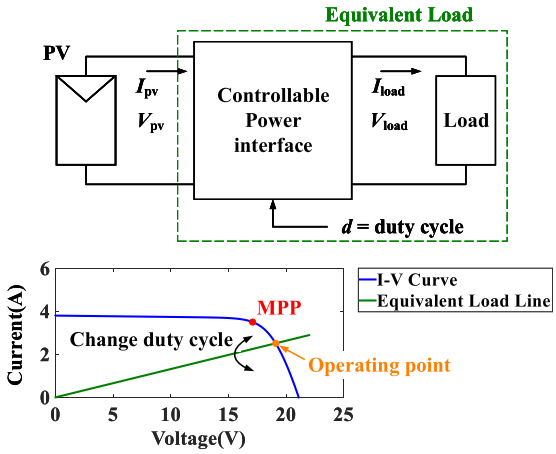

Fig. 4. Function of controllable power interfaces between the PV source and the load.

of MPPT algorithms for a practical PV system design. Thus, deep investigation for the EN50530 dynamic test procedure is highly demanded considering the rapid development of MPPT algorithms and the advantages of EN50530 dynamic test procedure. This article provides a comprehensive evaluation of several advanced MPPT algorithms in terms of their operating principles and performance evaluation under the EN50530 dynamic test procedure. In order to cover different irradiance changing conditions, two dynamic EN50530 test sequences are adopted for the performance evaluation. The effects of wrong-step changes by using three MPPT algorithms are analyzed systematically. An experimental comparison of three selected MPPT algorithms in terms of the tracking routines, accumulated energy, and tracking efficiency is presented.

II. Review of PV MPPT Algorithms

The basic principle behind MPPT algorithms is the impedance match between the PV source and the load, which will be accomplished by the controllable power interface [2]. As shown in Fig. 4, the controllable power interface and the load as a whole can be regarded as an equivalent load. Generally, dc–dc converters are used as the controllable power interface and the load can be either the resistive load or the batteries, which will be discussed separately.

When the resistive load is used, the corresponding mathematical expression can be derived as [2]

$$R_{\text{pv}} = \frac{R_{\text{load}}}{M(d)^2} \tag{1}$$

where R_{pv} and R_{load} represent the impedance of the PV source and the load, respectively. $M(d)$ is the voltage conversion ratio. If the boost converter is used as the controllable power interface, the corresponding $M(d)$ is given as

$$M(d) = \frac{V_{\text{load}}}{V_{\text{pv}}} = \frac{1}{1-d}. \tag{2}$$

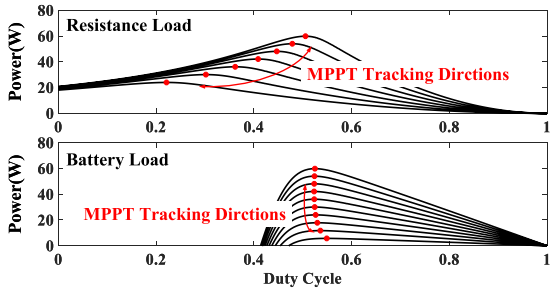

Fig. 5. Distribution of the MPPs under different types of load conditions.

Substitute (2) into (1), the relationship between R_{pv} and R_{load} can be derived as

$$R_{\text{pv}} = R_{\text{load}}(1-d)^2 \tag{3}$$

where the term $R_{\text{load}}(1-d)^2$ is the equivalent load and d refers to duty cycle. By changing the value of d, the equivalent load will be changed and the movement of operating points will be regulated accordingly.

Similarly, when the battery load is used, (2) can be rewritten as

$$V_{\text{pv}} = V_{\text{load}}(1-d). \tag{4}$$

Assuming the parameters of R_{load} and V_o are set as 20 Ω and 36 V, respectively, the corresponding P–D characteristic curves concerning the distribution of MPPs under different solar irradiance levels are demonstrated in Fig. 5. From Fig. 5, it can be seen that the distribution characteristics of the MPPs are strikingly different for two kinds of loads: the resistive load and the battery load. Specifically, for the resistive load, the locations of the MPPs are widely dispersed on the P–D characteristic curves with respect to the solar irradiance level. By contrast, the locations of the MPPs for the battery load are relatively gathered as an approximate linear line. Therefore, as illustrated in Fig. 5, the characteristic differences about the distribution of MPPs under different loads will significantly affects the MPPT tracking direction.

So far, many MPPT algorithms have been discussed [18], [63], [64]. Table II lists main MPPT algorithms with their characteristics. Considering that the dynamic characteristics of the listed MPPT algorithms under the stepped test procedure are mainly determined by two important control variables: MPPT perturbation step size and perturbation direction, therefore, the effects of the two control variables on the dynamic performance of the listed MPPT algorithms will be discussed here with details.

A. Two Basic MPPT Algorithms: P&O and INC

P&O and INC are the most popular MPPT algorithms [20]–[24]. In order to clearly present the inherent mechanism in determining the perturbation direction, the tracking principle of the P&O and INC is illustrated in Fig. 6. As shown in Fig. 6, the perturbation direction for both P&O and INC can be determined from the P–V characteristics of PV modules, which can be

TABLE II
COMPARISON OF MPPT ALGORITHMS WITH MAIN CHARACTERISTICS

Method	Category	Static Oscillations	Tracking Speed	Different Conditions	Drift Condition	Initial Points	Parameter Tuning	Control Difficulty	True MPP	References
FSS P&O and INC	FSS	Depends	Slow	Yes	Yes	No	Depends	Simple	Yes	[21–25]
VSS P&O and INC	VSS	Depends	Depends	Yes	Yes	No	Yes	Simple	Yes	[7–9, 26–32]
Drift-free P&O and INC	FSS VSS	Depends	Slow	Yes	No	No	Depends	Simple	Yes	[33–37]
Fuzzy Logic Control	VSS	Depends	Fast	Depends	Depends	No	Yes	Difficult	Yes	[38–46]
Parabolic Prediction	VSS	Depends	Slow	Depends	Depends	Yes	No	Difficult	Yes	[47–50]
I-V Curve Fitting	VSS	No	Fast	Depends	No	Yes	Yes	Depends	No	[51–55]
MPP-Locus	HSS	Depends	Fast	No	No	No	Yes	Depends	Yes	[56–59]
Beta	HSS	Depends	Fast	Depends	No	No	Yes	Depends	Yes	[60–66]

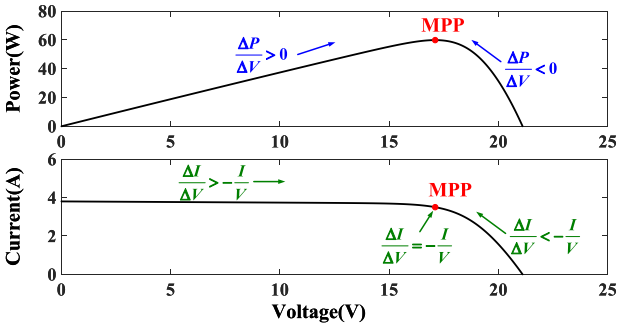

Fig. 6. Tracking principle of two classical algorithms.

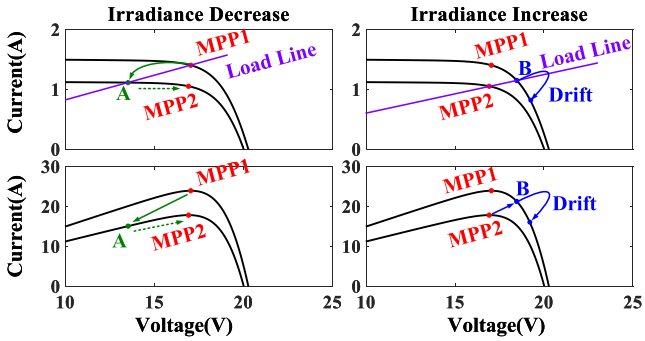

Fig. 7. Tracking details analysis under sudden irradiance changes.

expressed by

$$\text{P\& O}\begin{cases}\frac{\Delta P}{\Delta V}>0, & \text{Left of MPP} \quad (5a)\\ \frac{\Delta P}{\Delta V}<0, & \text{Right of MPP} \quad (5b)\end{cases}$$

$$\text{INC}\begin{cases}\frac{\Delta I}{\Delta V}>-\frac{I}{V}, & \text{Left of MPP} \quad (6a)\\ \frac{\Delta I}{\Delta V}=-\frac{I}{V}, & \text{At MPP} \quad (6b)\\ \frac{\Delta I}{\Delta V}<-\frac{I}{V}, & \text{Right of MPP} \quad (6c)\end{cases}$$

where ΔP, ΔV, and ΔI refer to the changes in power, voltage, and current, respectively.

Under normal operating conditions, both P&O and INC are able to make correct movements toward the MPP. Fig. 7 shows the tracking details when the solar irradiance is suddenly changed. Specifically, when the solar irradiance is decreased, the operating point will move from MPP_1 to point A. Then, the operating point will move toward the MPP_2. However, a wrong movement may be observed under a sudden increase in the solar irradiance. As shown in Fig. 7, the operating point moves from the MPP to point B when the solar irradiance is increased. At this time, considering that both (5a) and (6a) are satisfied, the operating point is perturbed to the left. Therefore, the wrong movement is made for both P&O and INC and the operating point is drifted away from the true MPP.

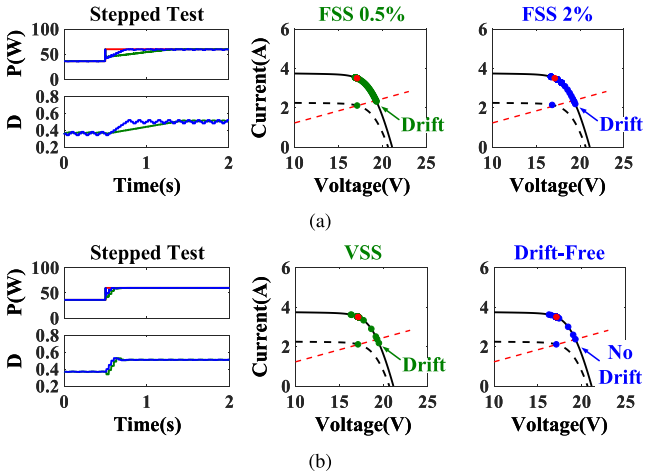

Fig. 8. Effects of the perturbation step size on the performance of P&O and INC under the stepped dynamic test procedure. (a) FSS method. (b) VSS and drift-free methods.

Fig. 8 illustrates the effects of the perturbation step size on the performance of P&O and INC under the stepped dynamic test

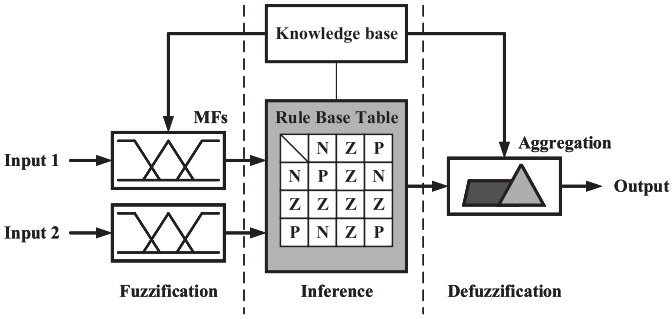

Fig. 9. Structure of the fuzzy logic controller.

procedure. It can be seen that the drift phenomenon may happen for both fixed-step size (FSS) and variable-step size (VSS) implementation of two MPPT methods. In order to avoid the drift phenomenon, one solution has been proposed in [34] and [35] by incorporating the information of ΔI in the determination for the algorithm perturbation direction. Since the drift phenomenon is normally happened during the irradiance increasing conditions, it is only required to incorporate ΔI in (5a) and (6a). Taking P&O method as an example, (5) can be rewritten as

$$\text{P\& O}\begin{cases}\frac{\Delta P}{\Delta V}>0 \quad \& \quad \Delta I<0, \text{Left of MPP} & \text{(7a)}\\ \frac{\Delta P}{\Delta V}>0 \quad \& \quad \Delta I>0, \text{Right of MPP} & \text{(7b)}\\ \frac{\Delta P}{\Delta V}<0, \quad \text{Right of MPP.} & \text{(7c)}\end{cases}$$

Fig. 8(b) demonstrates the movement of operating points by using the drift-free method. With the aid of ΔI, the drift-free operation can be accomplished for both two basic MPPT algorithms.

B. Fuzzy-Logic-Control (FLC)-Based MPPT Method

FLC is another popular MPPT method [37]–[45]. Generally, three stages are divided for the implementation of FLC-based MPPT methods, which are illustrated in Fig. 9. In the first stage, the numerical input variables are converted into equivalent linguistic variables, which are named as input fuzzy sets. In the second stage, the input fuzzy sets are converted into output fuzzy sets through the inference with the fuzzy rule base table. Finally, the output fuzzy sets are converted into the numerical variables as the output.

The FLC method generally exhibits good tracking performance. However, the drift phenomenon may also possibly happen, which are mainly dependent on the input parameters. As shown in Fig. 10, the error E and the change in error ΔE are used as the input parameters

$$E(k)=\frac{\Delta P}{\Delta V}=\frac{P(k)-P(k-1)}{V(k)-V(k-1)} \tag{8}$$

$$\Delta E(k)=E(k)-E(k-1) \tag{9}$$

where $P(k)$ and $V(k)$ are the PV output power and voltage at time k, respectively.

Fig. 10. Different input parameters for the FLC methods. (a) Type 1. (b) Type 2.

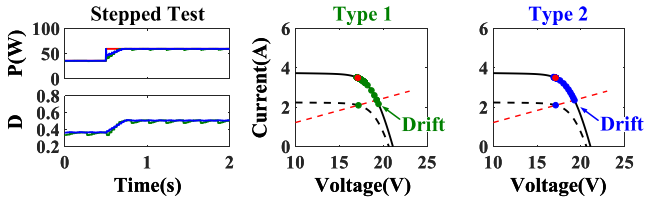

Fig. 11. Performance on two types of FLC methods under the stepped test procedure.

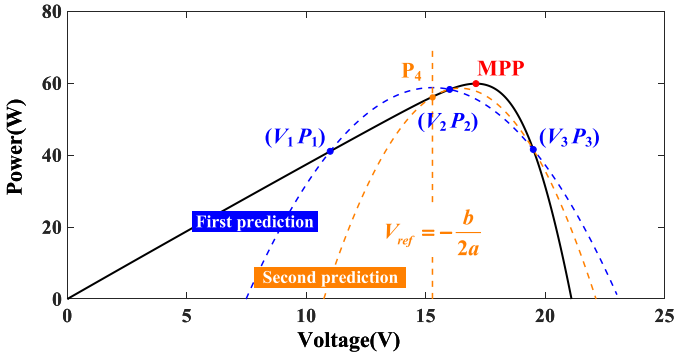

Fig. 12. Tracking principle of parabolic-prediction-based MPPT method.

For the type 2 FLC method, the second input parameter is replaced by

$$\Delta I(k)=I(k)-I(k-1) \tag{10}$$

where $I(k)$ refers to PV output current at time k.

Fig. 11 illustrates the performance on two types of FLC methods under the stepped dynamic test procedure. It can be seen that the type 1 FLC method will exhibit obvious drift from the MPP under the stepped change, whereas the type 2 FLC method will not.

C. Parabolic-Prediction-Based MPPT Method

Parabolic-prediction-based MPPT method is based on the fact that $P-V$ curves can be fitted by a parabolic curve [46]–[49]. As illustrated in Fig. 12, this method requires three points in the $P-V$ curve, namely (V_1 P_1), (V_2 P_2), and (V_3 P_3), to obtain the values of a, b, and c in a quadratic polynomial

$$P_{\text{pv}}=aV_{\text{pv}}^2+bV_{\text{pv}}+c. \tag{11}$$

Once these values are obtained, the operating point will move to the reference voltage V_{ref}

$$V_{\text{ref}}=-\frac{b}{2a}. \tag{12}$$

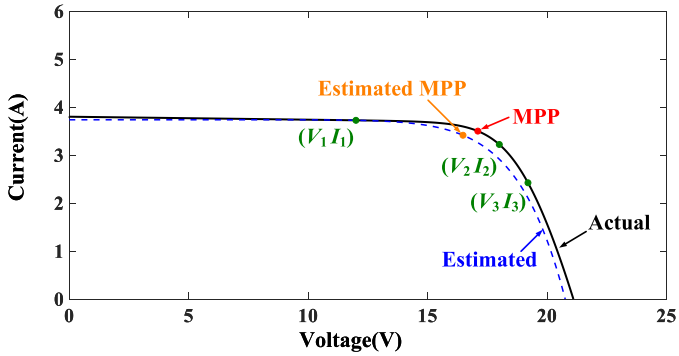

Fig. 13. Tracking principle of $I-V$ curve-fitting-based MPPT method.

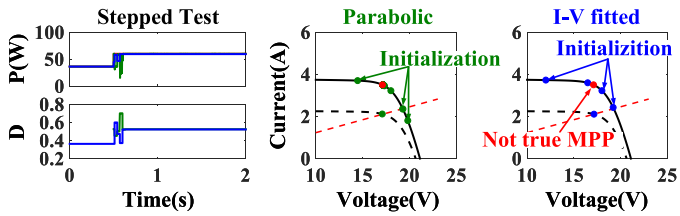

Fig. 14. Performance of the parabolic-prediction and $I-V$ curve-fitting-based MPPT methods under the stepped test procedure.

After the operating point moves to the new position, the corresponding power P_4 will be compared with P_1, P_2, and P_3. The lowest one will be dropped and the rest of points will be used for the next iteration. This iteration will be continuously repeated until the MPP is reached.

D. $I-V$ Curve-Fitting-Based MPPT Method

Similar to parabolic-prediction based method, $I-V$ curve-fitting-based method requires several pairs of voltage and current values in order to extract the physical parameters, such as R_s, R_p, and even the solar irradiance and temperature [50]–[54]. Taking [52] as an example, points (V_1 I_1), (V_2 I_2) and (V_3 I_3) are first measured, as shown in Fig. 13. Then, the points are used to obtain α, β, and γ in a simplified single-diode model as

$$I = \alpha + \beta V^{\gamma}. \tag{13}$$

Once α, β, and γ are obtained, the fitted $I-V$ curve as well as the MPP can be estimated. However, it should be noted that the estimated MPP by this method is not the true MPP.

Fig. 14 shows the performance on parabolic-prediction and $I-V$ curve-fitting-based MPPT methods under the stepped dynamic test procedure. The drift phenomenon will not likely happen for these two methods. However, it should be noted that the algorithm initialization is required for both methods.

E. MPP-Locus Method

MPP-locus method is one of typical hybrid step size (HSS) methods [55]–[58]. Generally, HSS-based MPPT methods have two stages: In the first stage, VSS is used to quickly allocate the MPP location. Then, in the second stage, FSS-based MPPT such as FSS P&O is used to track the exact location of the MPP.

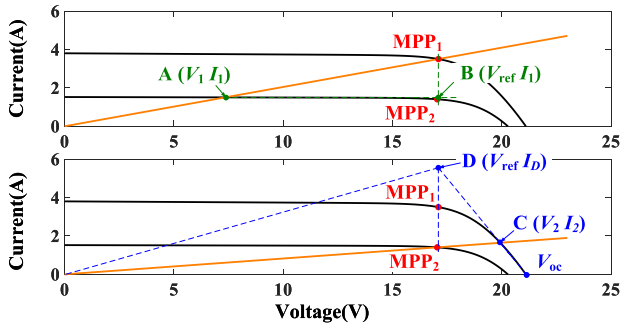

Fig. 15. Tracking principle of the MPP-locus method.

TABLE III
VALUES OF β UNDER VARIOUS IRRADIANCE AND TEMPERATURE

No.	Solar Irradiance	temperature	β
1	$1000W/m^2$	$45°C$	-15.4505
2	$1000W/m^2$	$5°C$	-18.3431
3	$300W/m^2$	$45°C$	-15.9587
4	$300W/m^2$	$5°C$	-19.0214

Specifically, the basic principle for MPP-locus MPPT method is originated from the fact that the locations of MPPs under different solar irradiance values are nearly form a straight line. Thus, once the operating point is shifted far from this straight line, the MPP-locus method will force it come back.

The tracking principle of the MPP-locus method is illustrated in Fig. 15 [58]. When the solar irradiance is decreased, the operating point moves from MPP_1 to point A (V_1, I_1). At this time, I_{mpp} can be approximately equal to I_1. Then, the operating point will be forced to B by using the MPP-locus algorithm. When the solar irradiance is increased, the operating point moves from MPP_2 to point C (V_2, I_2). Then, by applying the trigonometry rule, the following equation can be derived as

$$\frac{V_2 - V_{\text{mpp2}}}{I_D - I_2} = \frac{V_{\text{oc}}^* - V_{\text{mpp2}}}{I_D}. \tag{14}$$

Rearrange (14) and then I_D can be derived as

$$I_D = \frac{V_{\text{oc}}^* - V_{\text{mpp2}}}{V_{\text{oc}}^* - V_2} \times I_2 \tag{15}$$

F. Beta Method

Beta method is another HSS method. Unlike the aforementioned MPPT methods, an intermediate variable β is used to track the MPP. The basic principle of the beta method is illustrated in [59] and [60] and the intermediate variable β is expressed by

$$\beta = \ln\left(\frac{I_{\text{pv}}}{V_{\text{pv}}}\right) - c \times V_{\text{pv}} \tag{16}$$

where $c = q/(N_s \eta k T)$ is the diode constant.

First, the range of β, namely, β_{min} and β_{max}, depends on the working environment of the PV system. Table III demonstrates the determination of the range of β. The relationship among β, voltage, and power under various irradiation and temperature

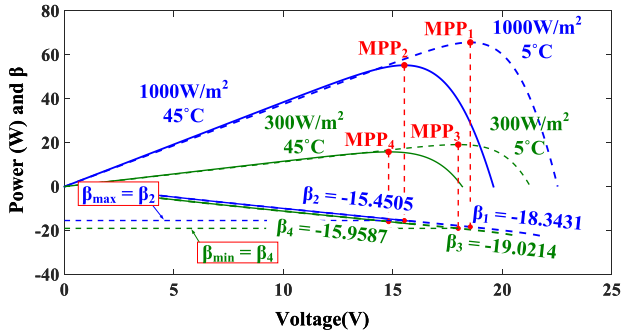

Fig. 16. Determination of β range based on the working environmental conditions.

TABLE IV
PARAMETERS SETTING FOR SEQUENCE A AND B

	n	Gradient, $W/m^2/s$	Pattern $(t_1/t_2/t_3/t_4)$	t_{ini}	Load (Ω)
A	10	50	(8/10/8/10)	30	80Ω
B	10	100	(7/10/7/10)	30	30Ω

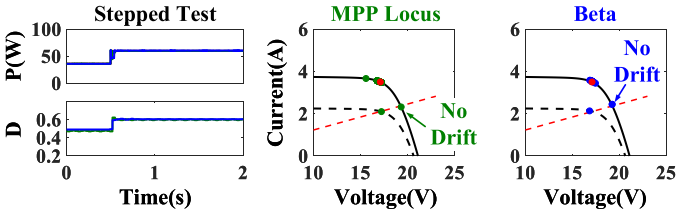

Fig. 17. Performance on MPP-locus and beta method under the stepped dynamic test procedure.

conditions is indicated in Fig. 16. From Table III and Fig. 16, the range of β is determined as: $\beta_{\min} = -19.02$ and $\beta_{\max} = -15.45$.

After that, the beta method will detect whether the value of β is within the set range of $[\beta_{\min}, \beta_{\max}]$. If the value of β is within the set range, it means that the operating point is close the MPP. Thus, the FSS P&O method can be used to exactly locate the MPP. Otherwise, if the value of β is out of the set range, it means that the operating point is far away from the MPP. Hence, a VSS ΔD is used, which can be expressed as

$$\Delta D = N \times (\beta(k) - \beta_g) \tag{17}$$

where $\beta(k)$ is the instantaneous value of β, N is the scaling factor, and β_g is a guiding parameter.

The beta method has been widely investigated and improved significantly in recent years [61]–[65]. It shows a very strong performance under various weather conditions, such as fast changing solar irradiance [63], [64] and partial shading condition [65]. Fig. 17 shows illustrates the performance on MPP-locus and beta method under the stepped dynamic test procedure. The drift phenomenon can be avoided for these two methods.

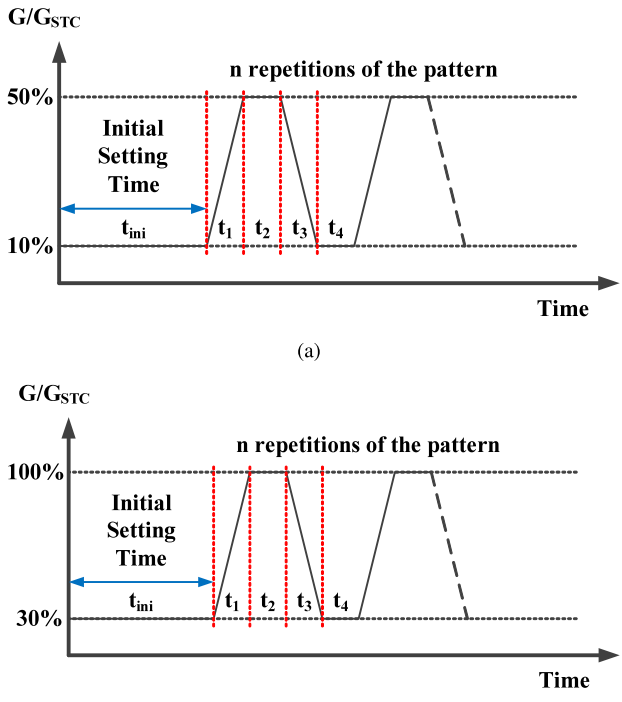

Fig. 18. Two sequences of EN50530 dynamic test procedure. (a) Sequence A. (b) Sequence B.

III. EN50530 DYNAMIC TEST PROCEDURE

A. EN50530 Dynamic Test Procedure

Fig. 18 illustrates two sequences of EN50530 dynamic test procedure with different irradiance levels: Sequence A features the irradiance fluctuation between 100 and 500 W/m^2, and Sequence B features the irradiance fluctuation between 300 and 1000 W/m^2 [10]. Table IV lists main parameters setting for Sequence A and B, where t_1, t_2, t_3, and t_4 represent the instants for the irradiance change and n represents the pattern repetition number.

Then, the expression for the dynamic efficiency is given by

$$\eta_{\text{dyn}} = \frac{\sum_i P_{\text{PV}} \cdot \Delta T_i}{\sum_j P_{\max} \cdot \Delta T_j} \tag{18}$$

where P_{PV} and ΔT_i refer to the actual output power and its duration, respectively, and $P_{\max}$ and ΔT_j represent the theoretical maximum power and the duration with $P_{\max}$, respectively.

B. PV Model Based on the EN50530 Procedure

In order to obtain a correct MPPT efficiency under EN50530 dynamic test procedure, the PV model for the PV simulator should be formulated.

The single-diode model is used as the comparative study considering it is the most commonly used for the PV modelling. The equivalent circuit of the single-diode model is shown in Fig. 19, which can be mathematically expressed by [66], [67]

$$I = I_{\text{ph}} - I_0 \left[\exp\left(\frac{V + IR_s}{N_s V_t} - 1 \right) \right] - \frac{V + IR_s}{R_{\text{sh}}} \tag{19}$$

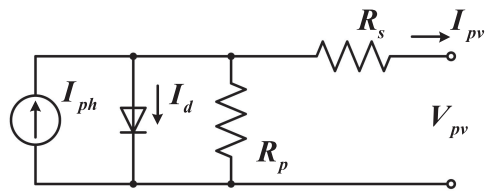

Fig. 19. Equivalent circuit of the single-diode model.

TABLE V
TECHNOLOGY-DEPENDENT PARAMETERS

	Unit	cSi-technology	Thin film technology
FF_V	[]	0.8	0.72
FF_I	[]	0.9	0.8
C_G	[W/m^2]	2,514E-03	1,252E-03
C_V	[]	8,593E-02	8,419E-02
C_R	[m^2/W]	1,088E-04	1,476E-04
α	[%/°C]	0.04	0.02
β	[%/°C]	-0.4	-0.2

where I and V refer to the output current and voltage, respectively from the PV module; I_{ph} is the PV current; I_0 is the reverse saturation current of the diode; R_s is the equivalent series resistance of the solar cell; R_{sh} is the equivalent shunt resistance; N_s is the number of the cells in the PV module; V_t is the junction thermal voltage which can be written as $V_t = \frac{kAT}{q}$, where q is the electron charge 1.602×10^{-19}C; A is the diode ideality factor; k is Boltzmann constant (1.38×10^{-23}J/K), and T (in K) is the temperature of the p-n junction. In (19), since the five parameters I_{ph}, A, I_0, R_s, and R_{sh} must be determined, this PV model is also known as the five-parameter PV model.

For the PV model based on the EN50530 dynamic test procedure, the relationship between I and V can be simplified, which is expressed by [68]

$$I = I_{\text{sc}} - I_0 \left[\exp\left(\frac{V}{V_{\text{oc}} C_{AQ}} - 1\right)\right] \tag{20}$$

where I_{sc} and V_{oc} are the short-circuit current and open-circuit voltage, respectively, which can be expressed by

$$I_{\text{sc}} = \frac{G}{G_{\text{stc}}} I_{\text{sc,stc}} \cdot [1 + \alpha \cdot (T - T_{\text{stc}})] \tag{21}$$

$$V_{\text{oc}} = V_{\text{oc,stc}} \cdot [1 + \beta \cdot (T - T_{\text{stc}})] \cdot \left[\ln\left(\frac{G}{C_G} + 1\right) \cdot C_V - C_R \cdot G\right] \tag{22}$$

where G represents the solar irradiance; $I_{\text{sc, stc}}$, $V_{\text{oc,stc}}$, T_{stc}, and G_{stc} are the corresponding parameters under the procedure test condition (STC); α, β, C_G, C_V, and C_R are constants, as shown in Table V. C_{AQ} in (20) is expressed by

$$C_{AQ} = \frac{\text{FF}_V - 1}{\ln(1 - \text{FF}_I)} \tag{23}$$

where FF_V and FF_I are the ratio of $V_{\text{mpp,stc}}$ to $V_{\text{oc,stc}}$ and $I_{\text{mpp,stc}}$ to $I_{\text{sc, stc}}$, respectively. I_0 is irradiance-dependent current, which is expressed by

$$I_0 = \frac{G}{G_{\text{stc}}} I_{\text{sc,stc}} \left(1 - \text{FF}_I\right)^{[1/(1-\text{FF}_V)].} \tag{24}$$

TABLE VI
MAIN PARAMETERS FOR MSX-60 W PV MODULES

Parameter	Value
Maximum power P_{mpp}	$59.85W$
Voltage at MPP V_{mpp}	$17.1V$
Current at MPP I_{mpp}	$3.5A$
Open-circuit voltage V_{oc}	$21.1V$
Short-circuit current I_{sc}	$3.8A$
Temperature coefficient of V_{oc}	$-80mV/°C$
Temperature coefficient of I_{sc}	$0.065\%/°C$

Table VI lists the main electrical parameters of the selected PV module MSX-60 W. The $P-V$ curve comparison between the EN50530 model and the single-diode model under Sequence A and B is shown in Fig. 20. It is clearly noticed that the $P-V$ curves by using the EN50530 model and the single-diode model exhibit significant differences, especially for the position of V_{oc}, the position for V_{mpp}, and the slopes of $P-V$ curves near the V_{oc}. Therefore, under the EN50530 dynamic test procedure, the performance evaluation of some classical MPPT algorithms, such as the $I-V$ fitted-curve method [58], MPP-locus method [55], [56] and VSS method [26], will be affected by the differences in PV models.

C. Effects of Wrong Step Changes for EN50530 Procedure

The effects of wrong step changes on the dynamic tracking performance of two classical algorithms, P&O and INC, have been studied in [34], [35], [69], and [70]. One or a small amount of wrong step changes will not affect the tracking performance of two MPPT algorithms too much under the sudden irradiance increasing condition [63], [64]. However, considering the operating conditions defined in the EN50530 dynamic test procedures, the accumulated effects of wrong step changes are not negligible with the continuous increase in the solar irradiance. Consequently, the divergence from the real MPP will eventually occur.

Fig. 21 illustrates the comparison of FSS P&O method with different step size and perturbation time (T_p) parameters under different ramp rate values. Here, T_p is defined as the time period between two successive perturbations. Generally, T_p should be longer than the transient setting time of PV power systems [20].

From Fig. 21, the ramp rate speed exhibits strong effect on the performance of the FSS P&O method. When the ramp rate speed is low such as 30 W/s, the FSS P&O method is capable of relocating the new MPP since the effect of wrong step change is negligible. The actual tracking routine of operating points will follow the trajectory from the bottom to the top, as shown in Fig. 21(a). However, when the ramp rate speed is high, the trajectory of operating point will be shifted to the right-hand side, as shown in Fig. 21(b) and (c). The corresponding reason is that the wrong tracking continuously occurs during the fast and continuous irradiance increasing period. Thus, the operating

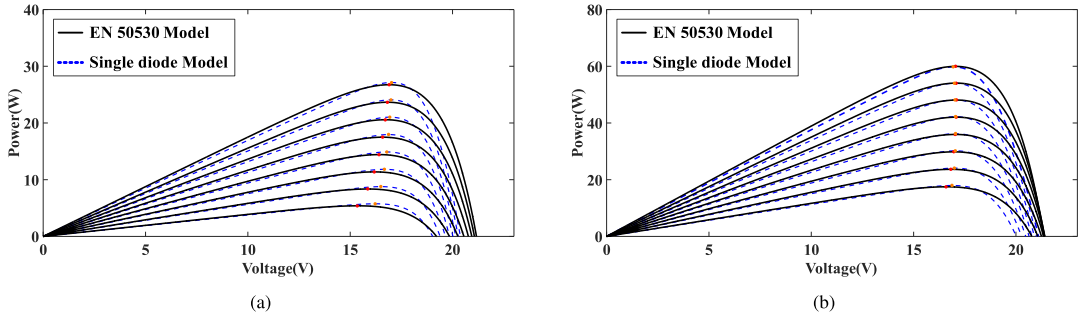

Fig. 20. Comparison of the $P-V$ curves between the EN50530 model and single diode model under (a) Sequence A and (b) Sequence B.

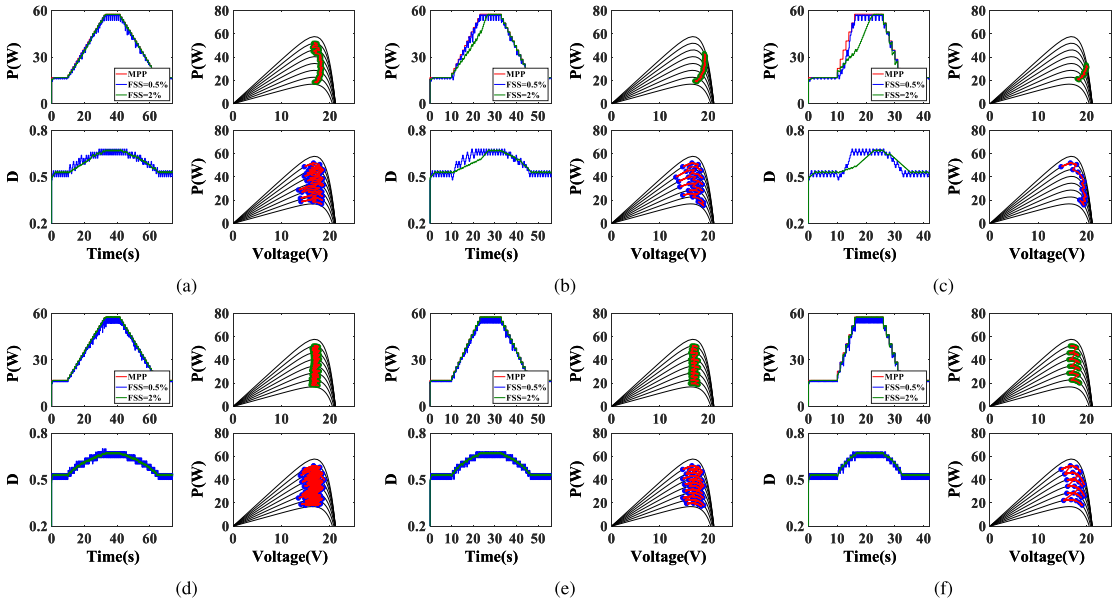

Fig. 21. Comparison of FSS P&O method with different step size and perturbation time (T_p) parameters under different ramp rate. (a) $T_p = 0.3$ s and ramp rate $= 30$ W/s. (b) $T_p = 0.3$ s and ramp rate $= 50$ W/s. (c) $T_p = 0.3$ s and ramp rate $= 100$ W/s. (d) $T_p = 0.1$ s and ramp rate $= 30$ W/s. (e) $T_p = 0.1$ s and ramp rate $= 50$ W/s. (f) $T_p = 0.1$ s and ramp rate $= 100$ W/s.

point is diverged from the real MPP, which adds more energy loss. Furthermore, the step size also affects the performance of FSS P&O method. Generally, a larger step size leads to a better dynamic performance but a worse steady-state performance. Apart from ramp the rate and step size, a lower value of T_p can also minimize the wrong step effect. As shown in Fig. 21(d)–(f), the FSS P&O method shows a good dynamic performance even with a small step size. However, it should be pointed that T_p is highly dependent on the system configuration. According to the work in[71], T_p in the CCR and the CVR can be derived by

$$T_p \geq T_\varepsilon \cong -\frac{1}{\zeta \cdot \omega_n} \cdot \ln\left(\varepsilon\sqrt{1-\zeta^2}\right) \tag{25}$$

where $\omega_n = 1/\sqrt{L \cdot C_{\text{in}}}$, $\zeta = 1/(2 \cdot R_{\text{pv}}) \cdot \sqrt{L/C_{\text{in}}}$, and $\varepsilon = 0.1$.

From the aforementioned tradeoff between the step size and perturbation time, it is not easy to minimize the effects of incorrect step changes. Therefore, it is essential for MPPT algorithms to avoid the drift phenomenon. Fig. 22 illustrates the tracking details analysis by using the beta method under the continuous irradiance increasing condition, which indicates that the beta method is capable of eliminating the effects of incorrect step changes caused by the continuous irradiance increase. Specifically, with fast irradiance increase, the operating point switches from MPP1 to B1 that is located out of the

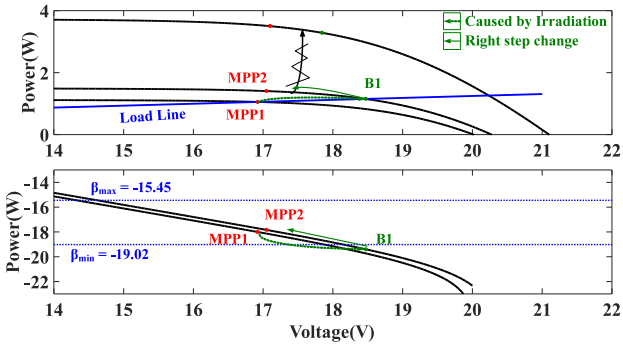

Fig. 22. Tracking details analysis of the beta method under the continuous irradiance increasing condition.

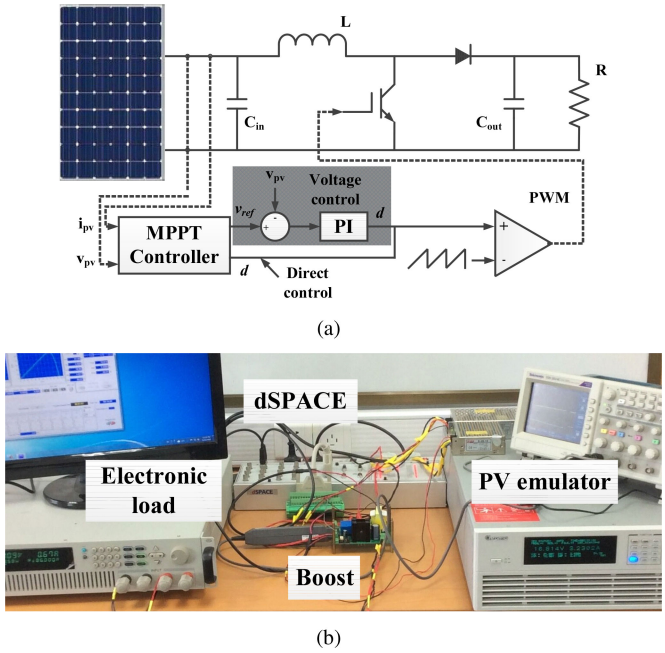

Fig. 23. (a) Schematic of the proposed PV test bench. (b) Experimental prototype.

set range of β. Then, the VSS mode of the Beta method will be triggered, which regulates the operating point move back toward the set range of β. The tracking routine by using the beta method under the continuous irradiance increasing condition will move like a sawtooth according to the inherent tracking mechanism. Thus, the effects of wrong step changes can be effectively eliminated [63].

IV. Experimental Results

In this section, the experimental results will be used to validate the aforementioned analysis. It can be seen that the drift phenomenon is a very serious problem for the EN50530 dynamic test procedure. Considering that the step size is acting as a key parameter related to the EN50530 dynamic test procedure; therefore, three typical MPPT algorithms, including an FSS P&O method, with 0.5% and 2%, the VSS INC method, and the HSS beta method are selected for the comprehensive dynamic comparison. Regarding the parabolic-prediction and $I-V$ curve-fitting-based MPPT methods, they are not selected for the comparison since they usually require several initial points, which are unable to response quickly to the fast ramp changes in solar irradiance.

A. System Setup

Fig. 23(a) and (b) shows the schematic of the proposed PV test bench and the corresponding experimental prototype, respectively. It consists of a PV panel, a dc–dc converter as the power interface, a resistive load and an MPPT controller. As shown in Fig. 23(a), the current $i_{\rm pv}$ and the voltage $v_{\rm pv}$ are sampled from the PV module as the inputs. Through different MPPT algorithms, the control variables such as the voltage reference or PWM pulses are generated as the outputs.

According to the control variable, MPPT algorithms can be implemented through two ways: direct MPPT control and indirect MPPT control. Regarding the indirect MPPT control, the output variables are the voltage or current reference, namely $v_{\rm ref}$ or $i_{\rm ref}$. Then, the actual PV output $v_{\rm pv}$ or $i_{\rm pv}$ will compare with $v_{\rm ref}$ or $i_{\rm ref}$. PI controller, as shown by the shaded areas in Fig. 23(a), is adopted to regulate the actual output to follow the reference generated by MPPT algorithms.

For the direct control, the PI control block is eliminated and the duty ratio D is generated as the output to generate the PWM pulses. Compared to the indirect MPPT control, the direct MPPT control can simplify the control structure and eliminate the tedious procedure for PI parameters. Therefore, the direct control is adopted for the MPPT implementation.

As shown in Fig. 23(b), the solar array emulator, Chroma ATE-62050H-600S, was used to simulate the PV module, MSX-60 W. For the boost converter, the main parameters are set as: the input capacitor $C_{\rm in}$ is 470μF, the output capacitor $C_{\rm out}$ is 47μF, the inductor L is 1mH, and the switching frequency is set as 10 kHz. dSPACE DS1104 is used to implement the MPPT algorithms and the perturbation time for the MPPT algorithm T_p is set as 0.3 s.

B. Experimental Results for EN50530 Dynamic Test Procedure

Main experimental power and voltage waveforms for two sequences of EN50530 dynamic test procedure are shown in Figs. 24 and 25, respectively. These results are recorded by the Chroma ATE-62050H-600S, where the red curves in Figs. 24 and 25 represent the theoretical maximum power $P_{\rm max}$ and the corresponding voltage $V_{\rm mpp}$ at $P_{\rm max}$, respectively.

Figs. 24 and 25 indicate that the P&O algorithm with 0.5% fix step size fails to track the MPP under both Sequence A and B, whereas the other algorithms are capable of achieving the function of MPPT under both sequences of EN50530 dynamic test procedure. The results show that the P&O algorithm with 2% step size has a fast convergence speed when the solar irradiance is continuously decreasing. However, it exhibits a slow convergence speed when the solar irradiance is continuously increasing. Similarly, the VSSINC algorithm exhibits a slow convergence speed under the irradiance increasing condition especially under the sequence A. However, the beta method shows fast convergence speeds for both sequences of EN50530 dynamic test procedure.

C. Tracking Routines Comparison on $P-V$ Curve

The tracking routines on the $P-V$ curve for the selected typical MPPT algorithms, including the P&O algorithm with FSS 0.5% and 2%, the VSSINC algorithm, and the beta method are illustrated in Figs. 26–29, respectively. Chroma ATE-62050H-600S is used to record the tracking data, which is ranging from 30 to 76 s and from 30 to 74 s for Sequence A and B, respectively.

The blue and green lines in these figures corresponds to the period with the irradiance increase and decrease, respectively.

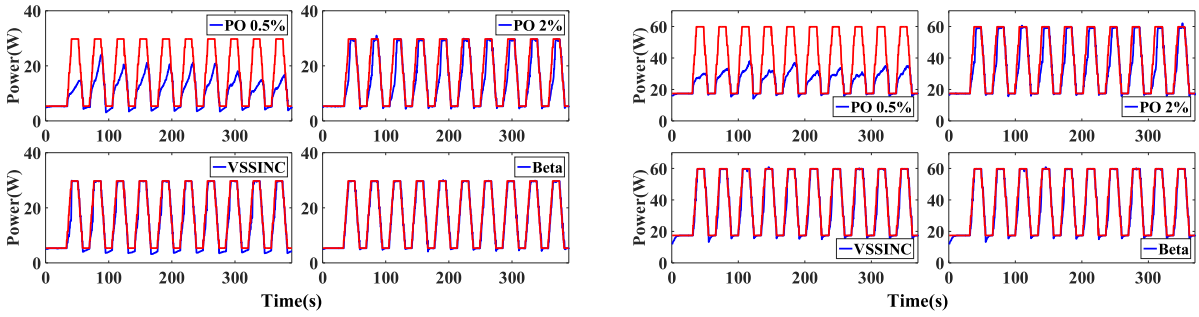

Fig. 24. Experimental power waveforms for selected typical MPPT methods under EN50530 dynamic test procedure. (a) Sequence A. (b) Sequence B.

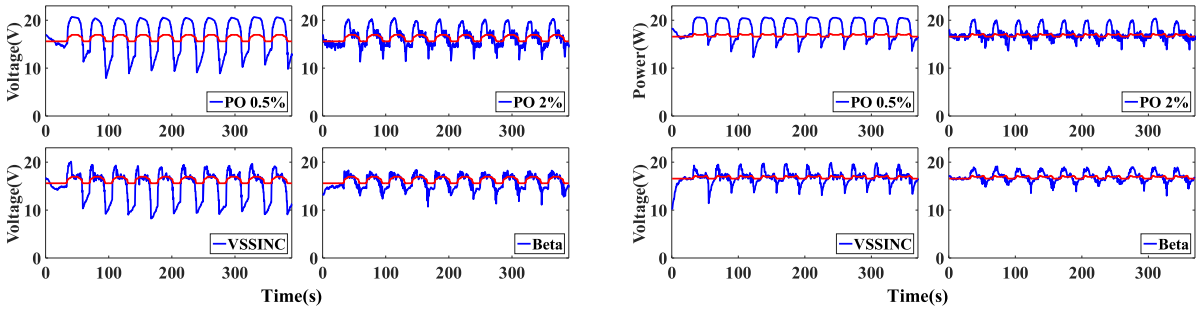

Fig. 25. Experimental voltage waveforms for selected typical MPPT methods under EN50530 dynamic test procedure. (a) Sequence A. (b) Sequence B.

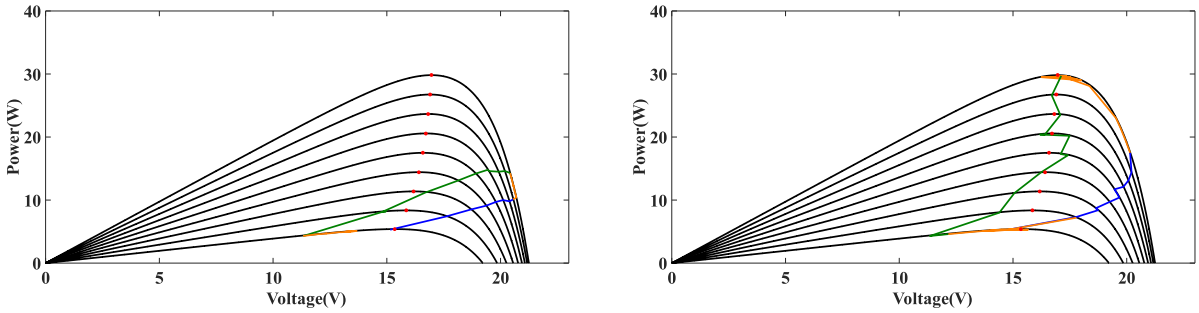

Fig. 26. $P-V$ tracking routines for the P&O algorithm with 0.5% step size. (a) Sequence A. (b) Sequence B.

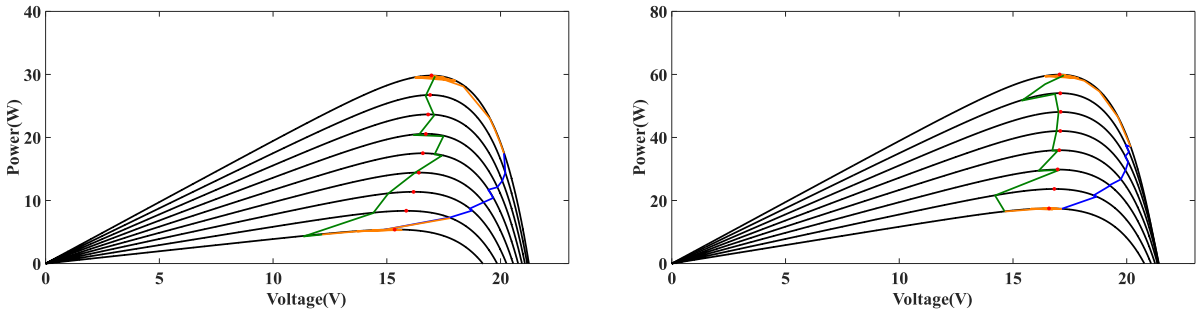

Fig. 27. $P-V$ tracking routines for the P&O algorithm with 2% step size. (a) Sequence A. (b) Sequence B.

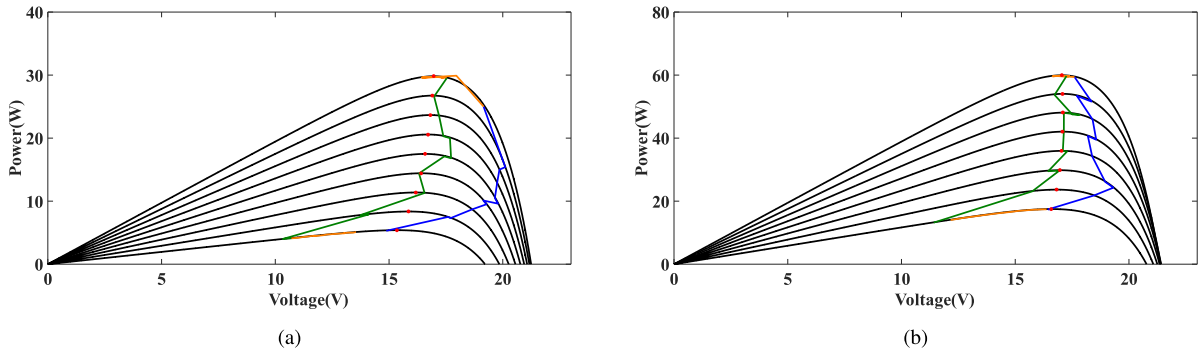

Fig. 28. $P-V$ tracking routines for the VSSINC algorithm. (a) Sequence A. (b) Sequence B.

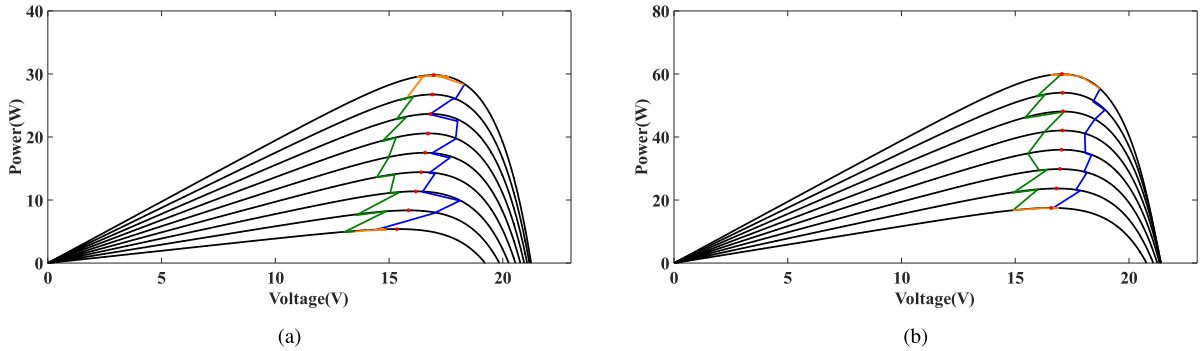

Fig. 29. $P-V$ tracking routines for the beta method. (a) Sequence A. (b) Sequence B.

The orange lines corresponds to the period when the irradiance stops to change. The red points refer to the real MPPs.

As shown in Fig. 26, the tracking routines by using the P&O algorithm with 0.5% step size are nearly a straight line when the irradiance is increasing, which is mainly caused by the accumulated wrong steps, as explained in Section III-C. Consequently, the operating point will gradually drift away from the true MPP. Considering the small step size, this algorithm will not have enough time to reach the MPP. Furthermore, this failure will significantly affect the next tracking period. The corresponding tracking routine for the next tracking period is also a straight line. Therefore, the tracking routines by using this algorithm looks like a circle slanted to the right.

With 2% step size, Fig. 27 illustrates that the tracking routine when the irradiance is increasing, which is also nearly a straight line. However, since its step size is large, this algorithm is able to track the MPP. Consequently, the next tracking period, marked as the green lines, will not be affected. Furthermore, since there is no wrong step change accumulated, most points on this tracking routine are close to the corresponding MPP. Therefore, with 2% rather than 0.5% step size, the dynamic tracking efficiency of the P&O algorithm has been significantly improved under EN50530 dynamic test procedure.

Similar to the P&O algorithm with 2% step size, the VSSINC method is also able to track the MPP when the irradiance is increasing, as shown in Fig. 28. Furthermore, since its step size can be automatically changed under the Sequence B according to the term $\Delta P/\Delta V$, the VSSINC method shows much better performance under the Sequence B than that under the Sequence A.

The tracking routine for the beta method is demonstrated in Fig. 29. Considering that there is no wrong step change during the period when the irradiance changes, the performance of the beta algorithm is much better than that of other three algorithms especially under the Sequence A. From Fig. 29, the overall tracking routines for the beta algorithm look like a sawtooth and the steady-state operating points are close to real MPPs.

D. Tracking Details Analysis

In order to make deep investigation on the tracking performance differences of these MPPT algorithms under EN50530 dynamic test procedure, the experimental tracking details are presented and analyzed. It should be noted that the period for the tracking details is mainly focused on the stage for the first irradiance increases after the initial setting time 30 s.

As shown in Fig. 30, the P&O algorithm with 0.5% will get perturbed around the load line, as previously discussed in Section III-C, Fig. 21 with ②. Consequently, the operating point will continuously drift away from the MPP during the period from 30 to 38 s for the Sequence A, and the period from 30 to 37 s for the Sequence B.

Subsequently, the P&O algorithm may drift too far away from the MPP and fail to track the MPP at 500 and 1000 W/m^2, respectively.

Fig. 31 shows that the experimental tracking details for the P&O algorithm with 2%. Unlike the case with 0.5% step size, the MPPT algorithm is able to track its MPP at both of 500 and 1000 W/m^2. However, the MPPT algorithm always exhibits

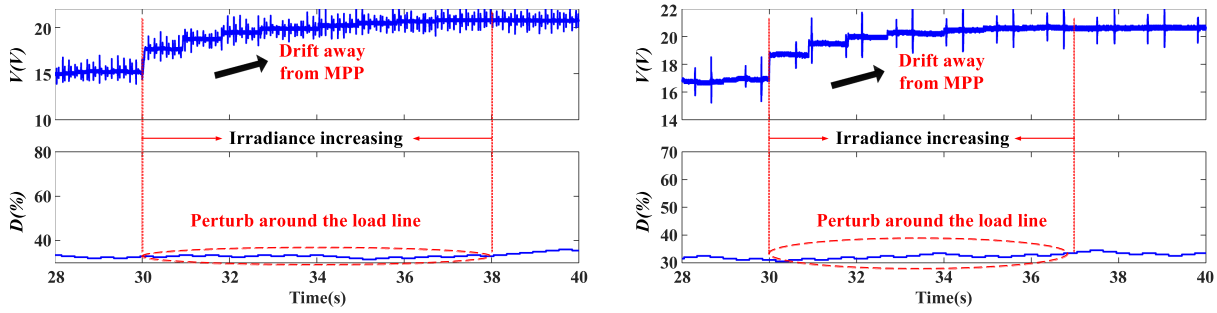

Fig. 30. Experimental tracking details for the P&O method with 0.5%. (a) Sequence A. (b) Sequence B.

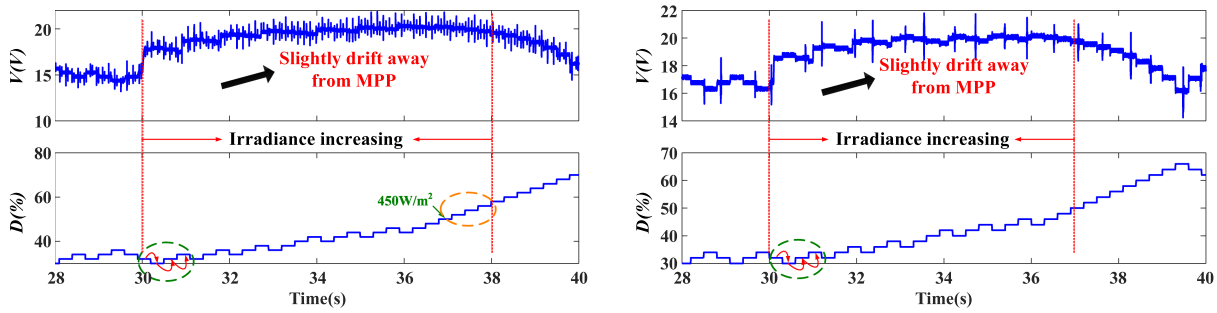

Fig. 31. Experimental tracking details for the P&O method with 2%. (a) Sequence A. (b) Sequence B.

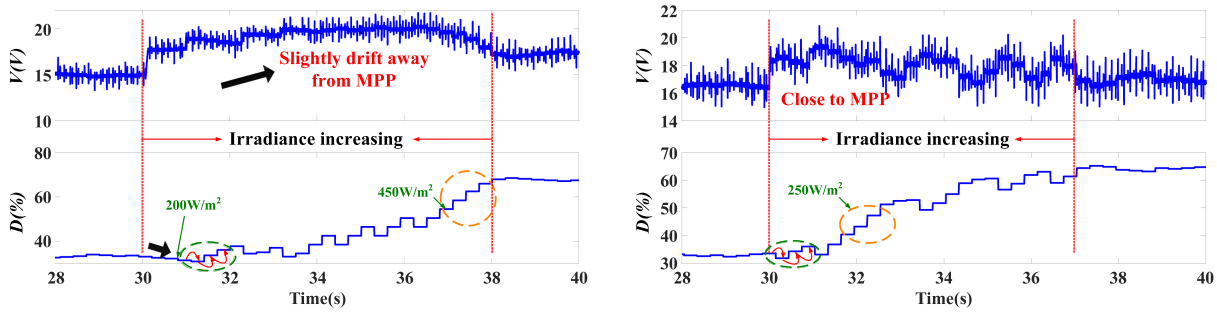

Fig. 32. Experimental tracking details for the VSSINC method. (a) Sequence A. (b) Sequence B.

obvious wrong step changes when the irradiance increases, and makes two another right step changes, as marked with a green circle and red arrows in Fig. 31. Consequently, the operating point will be slightly drifted away from the MPP during this period.

As shown in Fig. 32, the performance of the VSSINC algorithm is generally similar to that of the P&O algorithm with 2% step size especially under the sequence A. However, since the term $\Delta P/\Delta V$ in Sequence B is larger than Sequence A, the performance of the VSSINC method is much better than that of the P&O algorithm with 2% under the sequence B. Besides, during the period from 30 to 31 s for the Sequence A, the VSSINC algorithm makes continuous wrong step changes, as mark with a green arrow in Fig. 32(a), which affects the tracking performance of the VSSINC algorithm under the Sequence A.

The detailed tracking analysis by using the beta algorithm is illustrated in Fig. 33. Fig. 33 shows that the operating point is generally close to the MPP during the tracking period. The Beta algorithm can avoid the wrong step changes under the continuous irradiance increasing conditions. Furthermore, even though an unusual wrong steps change may happen as marked with green circles in Fig. 33(a) and (b), considering that these the operating points are still located within the β range as marked with green circles in Fig. 33(a) and (b), the effect on the tracking performance of Beta algorithm is negligible.

E. Evaluation

A comprehensive evaluation for experimental results under EN50530 dynamic test procedure is shown in Fig. 34. The

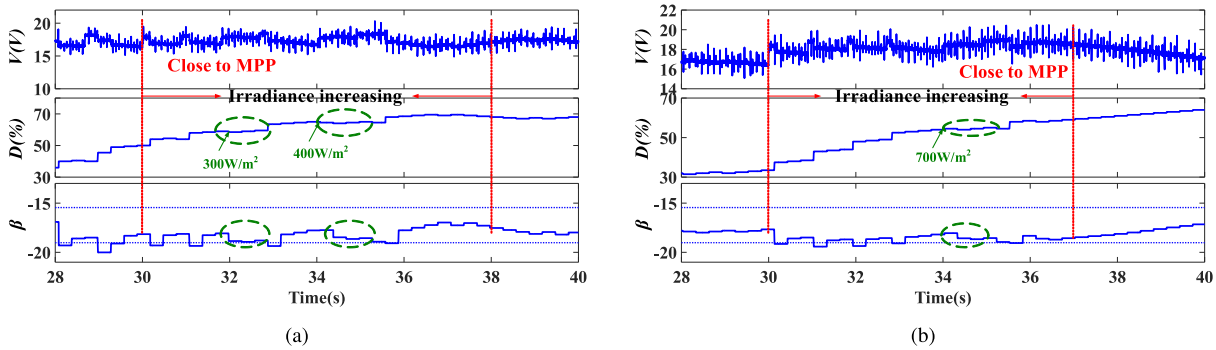

Fig. 33. Experimental tracking details for the beta method. (a) Sequence A. (b)Sequence B.

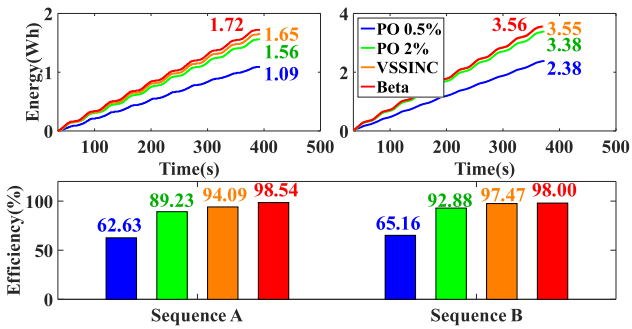

Fig. 34. Comparison of experimental results for EN50530 dynamic test procedure.

"Energy (W/h)" refers to the generated energy by the different MPPT algorithms, and "Efficiency (%)" is calculated by (18).

Fig. 34 shows that all these algorithm under the Sequence A exhibit relatively lower tracking efficiency than that under the Sequence B. As shown in Fig. 34, the P&O algorithm with 0.5% step size exhibits the lowest generated energy and efficiency due to the accumulated effects of wrong-step changes. Moreover, both the P&O algorithm and the VSSINC algorithms show deteriorated performance at the low irradiance level, whereas the beta method exhibits even better performance at the low irradiance level than that at the high level.

As illustrated in Fig. 34, the beta method always exhibit the highest generated energy and efficiency for either Sequence A or B.

V. Conclusion

In this article, after reviewing three dynamic test procedures, three typical MPPT algorithms, such as the FSS P&O, VSSINC, and HSS beta method, are evaluated comprehensively under the EN50530 dynamic test procedure. Two dynamic EN50530 test sequences are adopted for the performance evaluation to cover different irradiance changing conditions.

The experimental comparison of three MPPT algorithms in terms of the tracking routines, accumulated energy, and tracking efficiency is presented. The mechanism for the wrong step changes has been revealed, which account for the tracking drift phenomenon.

The research shows that the P&O with 0.5% FSS may fail to track the true MPP due to the tracking drift, whereas the beta algorithm exhibits the highest tracking efficiency under both dynamic sequences.

As a typical HSS MPPT algorithm, the beta method is capable of eliminating the effects of wrong step change, thus both the generated energy and the tracking efficiency by using the beta method are the highest among the selected MPPT algorithms. The experimental results shows that the generated energy by using the beta method shows 57.8% and 49.6% enhancement compared with that of the FSS P&O algorithm with 0.5% step size for two sequences of EN50530 dynamic test sequences, respectively. The measured efficiency is 98.54% and 98.00% by using the beta algorithm for the Sequence A and B. The average tracking efficiency improvement of the beta algorithm compared with other two tracking-success algorithms, namely FSS P&O algorithm with 2% step size and VSSINC, are experimentally measured as 24.2% and 18.8%, respectively.

References

[1] A. K. Podder, N. K. Roy, and H. R. Pota, "MPPT methods for solar PV systems: A critical review based on tracking nature," *IET Renewable Power Gener.*, vol. 13, no. 10, pp. 1615–1632, 2019.

[2] X. Li, Q. Wang, H. Wen, and W. Xiao, "Comprehensive studies on operational principles for maximum power point tracking in photovoltaic systems," *IEEE Access*, vol. 7, pp. 121407–121420, 2019.

[3] P.-C. Chen, P.-Y. Chen, Y.-H. Liu, J.-H. Chen, and Y.-F. Luo, "A comparative study on maximum power point tracking techniques for photovoltaic generation systems operating under fast changing environments," *Sol. Energy*, vol. 119, pp. 261–276, 2015.

[4] B. Peng, K. Ho, and Y. Liu, "A novel and fast MPPT method suitable for both fast changing and partially shaded conditions," *IEEE Trans. Ind. Electron.*, vol. 65, no. 4, pp. 3240–3251, Apr. 2018.

[5] Y. Hong, S. N. Pham, T. Yoo, K. Chae, K.-H. Baek, and Y. S. Kim, "Efficient maximum power point tracking for a distributed PV system under rapidly changing environmental conditions," *IEEE Trans. Power Electron.*, vol. 30, no. 8, pp. 4209–4218, Aug. 2015.

[6] Y. Wang, Y. Li, and X. Ruan, "High-accuracy and fast-speed MPPT methods for PV string under partially shaded conditions," *IEEE Trans. Ind. Electron.*, vol. 63, no. 1, pp. 235–245, Jan. 2016.

[7] W. Xiao, H. H. Zeineldin, and Z. Peng, "Statistic and parallel testing procedure for evaluating maximum power point tracking algorithms of photovoltaic power systems," *IEEE J. Photovolt.*, vol. 3, no. 3, pp. 1062–1069, Jul. 2013.

[8] I. Houssamo, F. Locment, and M. Sechilariu, "Experimental analysis of impact of MPPT methods on energy efficiency for photovoltaic power systems," *Int. J. Elect. Power*, vol. 46, pp. 98–107, 2013.

[9] Y. Du, X. Li, H. Wen, and W. Xiao, "Perturbation optimization of maximum power point tracking of photovoltaic power systems based on practical solar irradiance data," in *Proc. IEEE 14th Workshop Control Model. Power Electron.*, 2015, pp. 1–5.

[10] T. Andrejasic, M. Jankovec, and M. Topic, "Comparison of direct maximum power point tracking algorithms using EN 50530 dynamic test procedure," *IET Renewable Power Gener.*, vol. 5, no. 4, pp. 281–286, Jul. 2011.

[11] D. Sera, L. Mathe, T. Kerekes, S. V. Spataru, and R. Teodorescu, "On the perturb-and-observe and incremental conductance MPPT methods for PV systems," *IEEE J. Photovolt.*, vol. 3, no. 3, pp. 1070–1078, Jul. 2013.

[12] K. Ishaque, Z. Salam, and G. Lauss, "The performance of perturb and observe and incremental conductance maximum power point tracking method under dynamic weather conditions," *Appl. Energy*, vol. 119, pp. 228–236, 2014.

[13] J. Ahmed and Z. Salam, "A modified P&O maximum power point tracking method with reduced steady state oscillation and improved tracking efficiency," *IEEE Trans. Sustain. Energy*, vol. 7, no. 4, pp. 1506–1515, Oct. 2016.

[14] M. Metry, M. B. Shadmand, R. S. Balog, and H. Abu-Rub, "MPPT of photovoltaic systems using sensorless current-based model predictive control," *IEEE Trans. Ind. Appl.*, vol. 53, no. 2, pp. 1157–1167, Mar. 2017.

[15] R. B. A. Koad, A. F. Zobaa, and A. El-Shahat, "A novel MPPT algorithm based on particle swarm optimization for photovoltaic systems," *IEEE Trans. Sustain. Energy*, vol. 8, no. 2, pp. 468–476, Apr. 2017.

[16] A. Lashab, D. Sera, J. M. Guerrero, L. Mathe, and A. Bouzid, "Discrete model-predictive-control-based maximum power point tracking for PV systems: Overview and evaluation," *IEEE Trans. Power Electron.*, vol. 33, no. 8, pp. 7273–7287, Aug. 2018.

[17] A. Lashab, D. Sera, and J. M. Guerrero, "A dual-discrete model predictive control-based MPPT for PV systems," *IEEE Trans. Power Electron.*, vol. 34, no. 10, pp. 9686–9697, Oct. 2019.

[18] B. Subudhi and R. Pradhan, "A comparative study on maximum power point tracking techniques for photovoltaic power systems," *IEEE Trans. Sustain. Energy*, vol. 4, no. 1, pp. 89–98, Jan. 2013.

[19] J. Ahmed and Z. Salam, "A modified P&O maximum power point tracking method with reduced steady-state oscillation and improved tracking efficiency," *IEEE Trans. Sustain. Energy*, vol. 7, no. 4, pp. 1506–1515, Oct. 2016.

[20] N. Femia, G. Petrone, G. Spagnuolo, and M. Vitelli, "Optimization of perturb and observe maximum power point tracking method," *IEEE Trans. Power Electron.*, vol. 20, no. 4, pp. 963–973, Jul. 2005.

[21] A. Safari and S. Mekhilef, "Simulation and hardware implementation of incremental conductance MPPT with direct control method using CUK converter," *IEEE Trans. Ind. Electron.*, vol. 58, no. 4, pp. 1154–1161, Apr. 2011.

[22] M. A. Elgendy, B. Zahawi, and D. J. Atkinson, "Assessment of perturb and observe MPPT algorithm implementation techniques for PV pumping applications," *IEEE Trans. Sustain. Energy*, vol. 3, no. 1, pp. 21–33, Jan. 2012.

[23] M. A. Elgendy, B. Zahawi, and D. J. Atkinson, "Assessment of the incremental conductance maximum power point tracking algorithm," *IEEE Trans. Sustain. Energy*, vol. 4, no. 1, pp. 108–117, Jan. 2013.

[24] M. A. Elgendy, B. Zahawi, and D. J. Atkinson, "Operating characteristics of the P&O algorithm at high perturbation frequencies for standalone PV systems," *IEEE Trans. Energy Convers.*, vol. 30, no. 1, pp. 189–198, Mar. 2015.

[25] W. Xiao and W. Dunford, "A modified adaptive hill climbing MPPT method for photovoltaic power systems," in *Proc. IEEE 35th Annu. Power Electron. Spec. Conf.*, vol. 3, Jun. 2004, pp. 1957–1963.

[26] F. Liu, S. Duan, F. Liu, B. Liu, and Y. Kang, "A variable step size inc MPPT method for PV systems," *IEEE Trans. Ind. Electron.*, vol. 55, no. 7, pp. 2622–2628, Jul. 2008.

[27] Q. Mei, M. Shan, L. Liu, and J. Guerrero, "A novel improved variable step-size incremental-resistance MPPT method for PV systems," *IEEE Trans. Ind. Electron*, vol. 58, no. 6, pp. 2427–2434, Jun. 2011.

[28] Y.-T. Chen, Z.-H. Lai, and R.-H. Liang, "A novel auto-scaling variable step-size MPPT method for a PV system," *Sol. Energy*, vol. 102, pp. 247–256, 2014.

[29] S. K. Kollimalla and M. K. Mishra, "Variable perturbation size adaptive P&O MPPT algorithm for sudden changes in irradiance," *IEEE Trans. Sustain. Energy*, vol. 5, no. 3, pp. 718–728, Jul. 2014.

[30] J. Ahmed and Z. Salam, "An enhanced adaptive P&O MPPT for fast and efficient tracking under varying environmental conditions," *IEEE Trans. Sustain. Energy*, vol. 9, no. 3, pp. 1487–1496, Jul. 2018.

[31] Y. Yang and H. Wen, "Adaptive perturb and observe maximum power point tracking with current predictive and decoupled power control for grid-connected photovoltaic inverters," *J. Mod. Power Syst. Clean Energy*, vol. 7, no. 2, pp. 422–432, 2019.

[32] N. Dasgupta, A. Pandey, and A. K. Mukerjee, "Voltage-sensing-based photovoltaic MPPT with improved tracking and drift avoidance capabilities," *Sol. Energy Mater. Sol. Cells*, vol. 92, no. 12, pp. 1552–1558, 2008.

[33] A. Pandey, N. Dasgupta, and A. Mukerjee, "High-performance algorithms for drift avoidance and fast tracking in solar MPPT system," *IEEE Trans. Energy Convers.*, vol. 23, no. 2, pp. 681–689, Jun. 2008.

[34] T. K. Soon and S. Mekhilef, "Modified incremental conductance MPPT algorithm to mitigate inaccurate responses under fast-changing solar irradiation level," *Sol. Energy*, vol. 101, pp. 333–342, 2014.

[35] M. Killi and S. Samanta, "Modified perturb and observe MPPT algorithm for drift avoidance in photovoltaic systems," *IEEE Trans. Ind. Electron*, vol. 62, no. 9, pp. 5549–5559, Sep. 2015.

[36] X. Li, H. Wen, Y. Hu, and L. Jiang, "Drift-free current sensorless MPPT algorithm in photovoltaic systems," *Sol. Energy*, vol. 177, pp. 118–126, 2019.

[37] A. Messai, A. Mellit, A. M. Pavan, A. Guessoum, and H. Mekki, "FPGA-based implementation of a fuzzy controller (MPPT) for photovoltaic module," *Energy Convers. Manage.*, vol. 52, no. 7, pp. 2695–2704, 2011.

[38] B. N. Alajmi, K. H. Ahmed, S. J. Finney, and B. W. Williams, "Fuzzy-logic-control approach of a modified hill-climbing method for maximum power point in microgrid standalone photovoltaic system," *IEEE Trans. Power Electron.*, vol. 26, no. 4, pp. 1022–1030, Apr. 2011.

[39] A. Al Nabulsi and R. Dhaouadi, "Efficiency optimization of a DSP-based standalone PV system using fuzzy logic and dual-MPPT control," *IEEE Trans. Ind. Informat.*, vol. 8, no. 3, pp. 573–584, Aug. 2012.

[40] A. El Khateb, N. A. Rahim, J. Selvaraj, and M. N. Uddin, "Fuzzy-logic-controller-based SEPIC converter for maximum power point tracking," *IEEE Trans. Ind. Appl.*, vol. 50, no. 4, pp. 2349–2358, Jul./Aug. 2014.

[41] J. Lee and Y. Kim, "Sensorless fuzzy-logic-based maximum power point tracking control for a small-scale wind power generation systems with a switched-mode rectifier," *IET Renew. Power Gener.*, vol. 10, no. 2, pp. 194–202, 2016.

[42] S. Tang, Y. Sun, Y. Chen, Y. Zhao, Y. Yang, and W. Szeto, "An enhanced MPPT method combining fractional-order and fuzzy logic control," *IEEE J. Photovolt.*, vol. 7, no. 2, pp. 640–650, Mar. 2017.

[43] A. A. S. Mohamed, A. Berzoy, and O. A. Mohammed, "Design and hardware implementation of FL-MPPT control of PV systems based on ga and small-signal analysis," *IEEE Trans. Sustain. Energy*, vol. 8, no. 1, pp. 279–290, Jan. 2017.

[44] X. Li, H. Wen, Y. Hu, and L. Jiang, "A novel beta parameter based fuzzy-logic controller for photovoltaic MPPT application," *Renewable Energy*, vol. 130, pp. 416–427, 2019.

[45] M. Fannakh, M. L. Elhafyani, and S. Zouggar, "Hardware implementation of the fuzzy logic MPPT in an Arduino card using a Simulink support package for PV application," *IET Renewable Power Gener.*, vol. 13, no. 3, pp. 510–518, 2019.

[46] N. Femia, D. Granozio, G. Petrone, G. Spagnuolo, and M. Vitelli, "Predictive & adaptive MPPT perturb and observe method," *IEEE Trans. Aerosp. Electron. Syst.*, vol. 43, no. 3, pp. 934–950, Jul. 2007.

[47] F. Pai and R. Chao, "A new algorithm to photovoltaic power point tracking problems with quadratic maximization," *IEEE Trans. Energy Convers.*, vol. 25, no. 1, pp. 262–264, Mar. 2010.

[48] F. Pai, R. Chao, S. H. Ko, and T. Lee, "Performance evaluation of parabolic prediction to maximum power point tracking for PV array," *IEEE Trans. Sustain. Energy*, vol. 2, no. 1, pp. 60–68, Jan. 2011.

[49] B. Bijukumar, A. G. K. Raam, S. I. Ganesan, C. Nagamani, and M. J. B. Reddy, "MPPT algorithm for thermoelectric generators based on parabolic extrapolation," *IET Gener., Transmiss., Distrib.*, vol. 13, no. 6, pp. 821–828, 2019.

[50] J. M. Blanes, F. J. Toledo, S. Montero, and A. Garrigs, "In-site real-time photovoltaic I–V curves and maximum power point estimator," *IEEE Trans. Power Electron.*, vol. 28, no. 3, pp. 1234–1240, Mar. 2013.

[51] J. Teng, W. Huang, T. Hsu, and C. Wang, "Novel and fast maximum power point tracking for photovoltaic generation," *IEEE Trans. Ind. Electron.*, vol. 63, no. 8, pp. 4955–4966, Aug. 2016.

[52] M. J. Z. Zadeh and S. H. Fathi, "A new approach for photovoltaic arrays modeling and maximum power point estimation in real operating conditions," *IEEE Trans. Ind. Electron.*, vol. 64, no. 12, pp. 9334–9343, Dec. 2017.

[53] E. I. Batzelis, G. E. Kampitsis, and S. A. Papathanassiou, "Power reserves control for PV systems with real-time MPP estimation via curve fitting," *IEEE Trans. Sustain. Energy*, vol. 8, no. 3, pp. 1269–1280, Jul. 2017.
[54] M. A. Ghasemi, A. Ramyar, and H. Iman-Eini, "MPPT method for PV systems under partially shaded conditions by approximating I–V curve," *IEEE Trans. Ind. Electron.*, vol. 65, no. 5, pp. 3966–3975, May 2018.
[55] M. Sokolov and D. Shmilovitz, "A modified MPPT scheme for accelerated convergence," *IEEE Trans. Energy Convers.*, vol. 23, no. 4, pp. 1105–1107, Dec. 2008.
[56] V. V. R. Scarpa, S. Buso, and G. Spiazzi, "Low-complexity MPPT technique exploiting the PV module MPP locus characterization," *IEEE Trans. Ind. Electron*, vol. 56, no. 5, pp. 1531–1538, May 2009.
[57] Y.-H. Liu and J.-W. Huang, "A fast and low cost analog maximum power point tracking method for low power photovoltaic systems," *Sol. Energy*, vol. 85, no. 11, pp. 2771–2780, 2011.
[58] T. K. Soon and S. Mekhilef, "A fast-converging MPPT technique for photovoltaic system under fast-varying solar irradiation and load resistance," *IEEE Trans. Ind. Informat.*, vol. 11, no. 1, pp. 176–186, Feb. 2015.
[59] S. Jain and V. Agarwal, "A new algorithm for rapid tracking of approximate maximum power point in photovoltaic systems," *IEEE Power Electron. Lett.*, vol. 2, no. 1, pp. 16–19, Mar. 2004.
[60] S. Jain and V. Agarwal, "Comparison of the performance of maximum power point tracking schemes applied to single-stage grid-connected photovoltaic systems," *IET Elect. Power Appl.*, vol. 1, no. 5, pp. 753–762, 2007.
[61] X. Li, H. Wen, and C. Zhao, "Improved beta parameter based MPPT method in photovoltaic system," in *Proc. IEEE 9th Int. Power Electron. ECCE Asia Conf.*, Jun. 2015, pp. 1405–1412.
[62] X. Li, H. Wen, L. Jiang, E. G. Lim, Y. Du, and C. Zhao, "Photovoltaic modified β-parameter-based MPPT method with fast tracking," *J. Power Electron.*, vol. 16, no. 1, pp. 9–17, 2016.
[63] X. Li, H. Wen, L. Jiang, W. Xiao, Y. Du, and C. Zhao, "An improved MPPT method for PV system with fast-converging speed and zero oscillation," *IEEE Trans. Ind. Appl.*, vol. 52, no. 6, pp. 5051–5064, Nov. 2016.
[64] X. Li, H. Wen, L. Jiang, Y. Hu, and C. Zhao, "An improved beta method with auto-scaling factor for photovoltaic system," *IEEE Trans. Ind. Appl.*, vol. 52, no. 5, pp. 4281–4291, Sep. 2016.
[65] X. Li, H. Wen, Y. Hu, L. Jiang, and W. Xiao, "Modified beta algorithm for GMPPT and partial shading detection in photovoltaic systems," *IEEE Trans. Power Electron.*, vol. 33, no. 3, pp. 2172–2186, Mar. 2018.
[66] M. Villalva, J. Gazoli, and E. Filho, "Comprehensive approach to modeling and simulation of photovoltaic arrays," *IEEE Trans. Power Electron.*, vol. 24, no. 5, pp. 1198–1208, May 2009.
[67] S. Shongwe and M. Hanif, "Comparative analysis of different single-diode PV modeling methods," *IEEE J. Photovolt.*, vol. 5, no. 3, pp. 938–946, May 2015.
[68] *Overall Efficiency of Grid Connected Photovoltaic Inverters*, EN50530, May 2010.
[69] T. K. Soon and S. Mekhilef, "A fast-converging MPPT technique for photovoltaic system under fast-varying solar irradiation and load resistance," *IEEE Trans. Ind. Informat.*, vol. 11, no. 1, pp. 176–186, Feb. 2015.
[70] X. Li and H. Wen, "Evaluation of different maximum power point tracking techniques by using EN 50530 dynamic test standard," in *Proc. IEEE Power Electron., Drives, Energy Syst.*, 2016, pp. 1–6.
[71] J. Kivimki, S. Kolesnik, M. Sitbon, T. Suntio, and A. Kuperman, "Revisited perturbation frequency design guideline for direct fixed-step maximum power point tracking algorithms," *IEEE Trans. Ind. Electron*, vol. 64, no. 6, pp. 4601–4609, Jun. 2017.

Xingshuo Li (Member, IEEE) was born in Zhengzhou, China. He received the B.S. degree in computer science from Zhengzhou University, Zhengzhou, China, in 2012, the M.S. degree in sustainable energy technology with distinction from Xi'an Jiaotong-Liverpool University, Suzhou, China, in 2015, and the Ph.D. degree in electrical engineering from the University of Liverpool, Liverpool, U.K., in 2019.

He is currently with Nanjing Normal University, Nanjing, China. His research interests include digital control, power electronics, and power converters for photovoltaic.

Huiqing Wen (Senior Member, IEEE) received the B.S. and M.S. degrees from Zhejiang University, Hangzhou, China, in 2002 and 2006, respectively, and the Ph.D. degree from the Chinese Academy of Sciences, Beijing, China, in 2009, all in electrical engineering.

From 2009 to 2010, he was an Electrical Engineer with the GE (China) Research and Development Center Company, Ltd., Shanghai, China. From 2010 to 2011, he was an Engineer with the China Coal Research Institute, Beijing, China. From 2011 to 2012, he was a Postdoctoral Fellow with the Masdar Institute of Science and Technology, Abu Dhabi, UAE. In 2013, he joined the Electrical and Electronic Engineering Department, Xi'an Jiaotong-Liverpool University, Suzhou, China, where he is currently an Associate Professor. He has authored/coauthored more than 50 peer-reviewed technical papers in leading journals. His research interests include renewable energy, electric vehicle, power electronics, microgrid, and power semiconductor devices.

Dr. Wen is currently the Associate Editor for IEEE ACCESS, *International Journal of Photoenergy*, and *Journal of Power Electronics*.

Yihua Hu (Senior Member, IEEE) received the B.S. degree in electrical engineering and the Ph.D. degree in power electronics and drives from the China University of Mining and Technology, Xuzhou, China, in 2003 and 2011, respectively.

From 2011 to 2013, he was with the College of Electrical Engineering, Zhejiang University, Hangzhou, China, as a Postdoctoral Fellow. From 2013 to 2015, he was a Research Associate with the Power Electronics and Motor Drive Group, University of Strathclyde, Glasgow, U.K. From 2016 to 2019, he was a Lecturer with the Department of Electrical Engineering and Electronics, University of Liverpool, Liverpool, U.K. He is currently a Reader with the Department of Electronics Engineering, The University of York, York, U.K. He has authored/coauthored 100 papers in IEEE Transactions journals. His research interests include renewable generation, power electronics converters and control, electric vehicle, more electric ship/aircraft, smart energy system, and nondestructive test technology.

Dr. Hu is currently an Associate Editor for the IEEE TRANSACTIONS ON INDUSTRIAL ELECTRONICS, *IET Renewable Power Generation*, *IET Intelligent Transport Systems,* and *Power Electronics and Drives*.

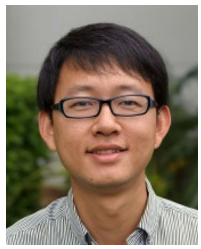

Yang Du (Member, IEEE) received the Ph.D. degree in electrical engineering from The University of Sydney, Sydney, NSW, Australia, in 2013.

From 2013 to 2014, he was with the Masdar Institute of Science and Technology, Abu Dhabi, UAE, as a Postdoctoral Research Fellow. From 2014 to 2018, he was a Lecturer with Xi'an Jiaotong-Liverpool University, Suzhou, China, where he maintains an honorary position. He joined James Cook University, Cairns, QLD, Australia, in 2019. He was a Visiting Scientist with the Massachusetts Institute of Technology, Cambridge, MA, USA, in 2018. His research interest includes solar forecasting, renewable energy integration, power electronics and smart grid.

Dr. Du is currently an Associate Editor for *IET Renewable Power Generation*.

Yong Yang (Senior Member, IEEE) received the B.S. degree in automation from Xiangtan University, Xiangtan, China, in 2003, the M.S. degree in electrical engineering from Guizhou University, Guiyang, China, in 2006, and the Ph.D. degree in electrical engineering from Shanghai University, Shanghai, China, in 2010.

He is currently an Associate Professor with the School of Rail Transportation, Soochow University, Suzhou, China. From 2017 to 2018, he was a Visiting Scholar with the Center for High Performance Power Electronics, The Ohio State University, Columbus, OH, USA. He has coauthored more than 60 journal and conference papers. His current research interests include model predictive control in power electronic converters, distributed energy resource interfacing, and high-performance motor drive control.